

# MODIFICATION OF THE EXTENDED TUBE MODEL (METM) FOR THE CHARACTERIZATION OF FILLED VULCANIZATES

CLAUS WRANA,<sup>1,\*</sup> ROBERT EBERLEIN<sup>2</sup>

<sup>1</sup>COMPOUNDS AG, PFÄFFIKON, SWITZERLAND

<sup>2</sup>ZHAW-IMES, WINTERTHUR, SWITZERLAND

RUBBER CHEMISTRY AND TECHNOLOGY, Vol. 97, No. 3, pp. 205–224 (2024)

## ABSTRACT

The aim of this study is to develop a material model for filled vulcanizates that is physically justifiable. This model builds upon the established extended tube model and is incorporated into a finite element program. The research demonstrates that the intrinsic deformation concept is inadequate for describing nonlinear deformation behavior under the assumption of incompressible, isotropic materials. Consequently, an alternative approach is proposed, employing a strain function rather than direct use of principal strains, to characterize reinforcement behavior. This strain function aligns with the first invariant of the right Cauchy-Green strain tensor over a wide deformation range. At minor deformations, the entanglements' contribution is considered through an additional reinforcement term. The novel reinforcement function is depicted as a sum of three elements, each representing reinforcement at different strain levels: low, medium, and high. Experimental comparisons show that the Modified Extended Tube Model (METM) effectively captures the stress-strain response of filled systems across all deformation levels. Furthermore, the reinforcement function parameters, derived from fitting the METM to experimental data, offer a quantitative assessment of the fillers' reinforcing effects, while the extended tube model parameters reflect the network characteristics. [doi:10.5254/rct.24.00021]

## INTRODUCTION

Due to their special mechanical properties, which can be customized by combining chemical and physical properties, rubber materials are indispensable in many technical applications today. The optimization of properties of elastomeric systems has therefore been intensively pursued in many fields, such as polymer chemistry, polymer physics, numerical mechanics and calibration techniques. It is an ongoing field of research with recent publications by e.g. Anssari-Benam et al.,<sup>1</sup> Costecalde et al.,<sup>2</sup> or Wan et al.,<sup>3</sup> to name just a few.

A fundamental aspect concerns the constitutive characterization of elastomeric materials. Over the past few decades, a multitude of formulations have been proposed (refer to, for instance, Bergström<sup>4</sup> for a comprehensive theoretical overview and Dal et al.<sup>5</sup> as well as He et al.<sup>6</sup> for recent reviews on the subject). Many of these approaches represent sophisticated phenomenological formulations for the strain energy function, while only a handful of models are grounded in physical principles, specifically the molecular structure of the material.

Heinrich and Kaliske<sup>7,8</sup> presented an extended approach of the “tube model”, which allows the characterization of the mechanical behavior at large deformations due to quantitative description of the finite extensibility of polymer chains. The extended tube model has been implemented in finite elements and enables the calculation of complex deformations of whole components based on molecularly defined network parameters as already assessed by Marckmann and Verron.<sup>9</sup> However, the extended tube model can currently only be used for unfilled polymer networks. In practice, filled, cross-linked elastomers are used almost exclusively due to their superior property profile. The simulation of the mechanical properties of filled systems with commercially available programs such as Abaqus<sup>10</sup> or Ansys<sup>11</sup> is usually carried out using purely empirically motivated model approaches. These include the Neo

\*Corresponding author. email: claus.wrana@compounds.ch

Hooke<sup>12</sup> model, the models from Mooney-Rivlin,<sup>13,14</sup> Ogden,<sup>15</sup> Yeoh<sup>16</sup> and several others. A good summary can be found at Bergström.<sup>4</sup> If the parameters of the respective models are carefully determined, the results of the simulations are usually very close to the real process. The finite element simulation is therefore a valuable and indispensable tool for the rapid and cost-sensitive development of elastomeric components. The primary drawback of these empirically motivated models is the inability to establish a correlation between the molecular properties of filled, cross-linked elastomers and the properties of the components manufactured from them. This implies that the outcomes of a finite element simulation can only be indirectly applied to compound formulation or optimization.

Vilgis et al.<sup>17</sup> developed an initial physically motivated model for filled systems, the so-called dynamic flocculation model which is predicated on the fractal characteristics of fillers. This model was subsequently refined and incorporated into finite element analysis by Klüppel and Schramm.<sup>18</sup> An alternative approach from Lorenz et al.<sup>19</sup> is based on the methods representative directions.

In this work, we present a novel methodology for analyzing polymer-filler interactions, predicated on a modification of the Extended Tube Model (ETM) by incorporating a deformation-dependent reinforcement function. This advancement can be viewed as an extension of the framework proposed by Heinrich and Vilgis.<sup>20</sup>

Our method distinguishes itself from existing approaches by extracting the deformation-dependent reinforcement directly from measurements, thereby obviating the need for predefined models such as the dynamic flocculation model.

Additionally, we introduce an analytical representation of the reinforcement function, with parameters that uniquely characterize the interactions between the filler and the polymer network, whereas those of the extended tube model encapsulate the network properties. This approach facilitates a quantitative differentiation between network properties and filler-filler and filler-polymer interactions. We will elucidate how the Extended Tube Model, when augmented with a reinforcement term, can be seamlessly integrated into finite element analysis programs. This integration establishes a direct link between the microstructural components of a filled polymer network and its resultant mechanical and dynamic-mechanical behaviors.

#### POLYMER PHYSICAL BACKGROUND

Heinrich and Kaliske<sup>8</sup> derived the strain energy for the extended tube model as a function of the chemical network density and the entanglements. They obtained the following expression

$$w = w_c + w_e = \frac{G_c}{2} \left[ \frac{(1 - \delta^2)(D_2 - 3)}{1 - \delta^2(D_2 - 3)} + \ln(1 - \delta^2(D_2 - 3)) \right] + \frac{2G_e}{\beta^2} (D_{-\beta} - 3) \quad (1)$$

for the energy density where

$$D_k = \sum_{i=1}^3 \lambda_i^k \quad (2)$$

$\lambda_i$  represents the principal stretches with  $i = 1, 2, 3$ .  $G_c$  is proportional to the chemical network density and  $G_e$  to the entanglement density. The parameter  $\delta$  describes the finite extensibility of chain segments between adjacent chemical cross-links. If an infinite extensibility is assumed,  $\delta = 0$  and Eq. 1 is reduced to Neo-Hooke's relation.  $D_k$  corresponds for  $k = 2$  to the 1<sup>st</sup> invariant of the right Cauchy-Green tensor  $\mathbf{C}$ . For  $k = -\beta$ ,  $D_k$  is utilized to characterize the

contribution of the entanglements to the deformation of the network. The parameter  $\beta$  ( $0 \leq \beta \leq 1$ ) was introduced to consider the global rearrangements of cross-links upon deformation<sup>21</sup> and, as a result, the release of topological constraints. Heinrich and Kaliske<sup>8</sup> used the data from Treloar<sup>12</sup> to show that a value of  $\beta = 0.2$  is best suited to describe the mechanical properties of vulcanized natural rubber.

If incompressibility  $J = \prod_{i=1}^3 \lambda_i = 1$  is assumed, the principal components of the stress  $\sigma_i$  can be calculated using Eq. 3. In most literature, the undeformed cross-sectional area is used to calculate the engineering stress  $P_i$  (1<sup>st</sup> Piola-Kirchhoff stresses).  $\sigma_i$  denote the true principal stresses (Cauchy stresses).

$$P_i = \frac{\partial w}{\partial \lambda_i} = \sigma_i \cdot \lambda_i^{-1}. \quad (3)$$

A first description of reinforcing properties of the filler were derived by Guth and Gold<sup>22</sup> by extending the hydrodynamic reinforcement.<sup>23,24</sup> A general description of the reinforcing properties of fillers is obtained by introducing a reinforcing function  $v(\Phi)$  where  $\Phi$  denotes the volume fraction of the filler.

$$E(\Phi) = E_0 \cdot v(\Phi) \quad (4)$$

where  $v(\Phi) = 1 + 2.5 \Phi + 14.1 \Phi^2$ . Domurath et al.<sup>25</sup> demonstrated that the value of 14.1 in the quadratic term is only valid under special conditions. They suggested a more general approach where  $v(\Phi) = 1 + 2.5 \Phi + b \Phi^2$ . The parameter  $b$  then depends on the matrix material as well as on the applied deformation.

Nonetheless, Eq. 4 only applies in the linear deformation range, i.e. in the limiting case of small deformations ( $\lambda \rightarrow 1$ ). In order to use Eq. 4 also for larger deformations, several authors<sup>4,26,27</sup> have introduced the intrinsic deformation approach.<sup>28</sup> In the concept of intrinsic deformation, it is assumed that the filler cannot be deformed. The deformation of the chains in the filled system  $\Lambda_i$  is then greater than the macroscopic deformation  $\lambda_i$ .

$$\Lambda_i - 1 = (\lambda_i - 1) \cdot v(\Phi) \quad (5)$$

However, this concept can only be used to a limited extent to describe the behavior of filled systems at larger deformations. The reason for this is that larger macroscopic deformations can cause negative deformations of the polymer chains  $\Lambda$  if isotropic and incompressible behavior is assumed. This becomes plausible if one considers the special case of uniaxial deformation of an isotropic and incompressible medium. For an elongation in the z-direction, the relation between the macroscopic deformation  $\lambda_z$  of the sample and the intrinsic deformation  $\Lambda_z$  of the polymer chains is described by Eq. 6 and Eq. 7.

$$\Lambda_z - 1 = (\lambda_z - 1) \cdot v(\Phi) \quad (6)$$

$$\Lambda_{x,y} - 1 = (\lambda_{x,y} - 1) \cdot v(\Phi) \quad (7)$$

Applying the assumption of incompressibility

$$\lambda_x \cdot \lambda_y \cdot \lambda_z = 1 \quad (8)$$

and isotropic behavior

$$\lambda_y = \lambda_x \quad (9)$$

and combining this with Eq. 6 and Eq. 7, we can derive the deformation  $\lambda_z$  at which the deformations  $\Lambda_x$  and  $\Lambda_y$  become less than zero.

$$\lambda_z > \left( \frac{v(\Phi)}{v(\Phi) - 1} \right)^2 \quad (10)$$

This cannot be realized, as even  $\Lambda_i = 0$  would require infinite compression. Negative deformations of the polymer chains in filled systems could be avoided either by an additional microscopic deformation condition or by abandoning the assumption of isotropic material behavior. Neither approach is physically justifiable, as to our knowledge there are no experimental findings that could justify such an approach.

#### ANALYTICAL DERIVATION OF THE STRAIN ENERGY DENSITY FUNCTION

We therefore propose a different approach, which we believe makes more physical sense. In our approach, the strain is no longer amplified, but the strain function  $D_k$  (see Eq. 1).

$$\tilde{D}_k - 3 = v(\Phi, D_k) (D_k - 3) \quad (11)$$

On the one hand, this approach prevents the strain from becoming negative; on the other hand, it leads to the reinforcement behavior described in Eq. 4 for the limiting case of small deformations (see Eq. 20). This approach is already present in Bergström's thesis.<sup>28</sup> However, it introduces only a constant reinforcement function that depends solely on the volume fraction of filler. We expand upon Bergström's approach by making the reinforcement function explicitly dependent on the strain function  $v(\Phi, D_k)$  and the volume fraction of the filler.

The great advantage over the existing empirical models is that our approach allows the separation of the filler-based effects from the nonlinear properties of the network by introducing a strain-dependent reinforcement function.

A combination of Eq. 1 and Eq. 11 leads to the strain energy function of a filled network. Eq. 12 shows the modified strain energy function of a filled network

$$\begin{aligned} w(\Phi) &= w_C(\Phi) + w_e(\Phi) \\ &= \frac{G_C}{2} \left[ \frac{(1 - \delta^2)v(\Phi, D_2)(D_2 - 3)}{(1 - \delta^2v(\Phi, D_2)(D_2 - 3))} + \ln(1 - \delta^2v(\Phi, D_2)(D_2 - 3)) \right] \\ &\quad + \frac{2G_e}{\beta^2} v(\Phi, D_{-\beta})(D_{-\beta} - 3) \end{aligned} \quad (12)$$

The deformation-dependent reinforcement function  $v(\Phi, D_k)$  can be determined experimentally. For this purpose, stress-strain measurements have to be carried out under different conditions (uniaxial, biaxial, and planar) for the filled and the unfilled system. It was shown experimentally<sup>29</sup> that fillers and in particular carbon black do not influence the cross-linking density of the network. For this reason, the reinforcement function can be determined for each deformation by minimizing the squared difference between the measured strain energy  $w_M(\Phi)$  and the strain energy function  $w_T(\Phi)$  calculated with Eq. 12. For this purpose, the parameters  $G_C$ ,  $G_e$ ,  $\delta$ , and  $\beta$  are determined from the stress-strain curve of the unfilled system. These values are then used to calculate the strain energy function  $w_T(\Phi)$  of the filled systems. In the next step, the strain energy  $w_M(\Phi)$  is calculated from the measured stress-strain curves (under uniaxial, biaxial or planar conditions) by a numerical integration.

For each deformation  $\lambda$ , the value of the reinforcement function  $v(\Phi, D_k)$  is now varied until the minimum of the least square root of the measured strain energy density  $w_M(\Phi)$  and the calculated energy density  $w_T(\Phi)$  is reached. In the experimental part, the numerical determination of the reinforcement function  $v(\Phi, D_k)$  is demonstrated using the example of two carbon blacks (N550 and N220) and four filler levels each.

ANALYTICAL DERIVATION OF THE PRINCIPAL STRESSES  $P_i$

The principal engineering stresses  $P_i$  can be calculated from Eq. 12 and Eq. 3. With the abbreviations

$$v_k = v(\Phi, D_k) \quad \text{and} \quad \dot{v}_k = \frac{\partial v(\Phi, D_k)}{\partial D_k} \tag{13}$$

one obtains

$$\begin{aligned} P_i &= P_{Ci} + P_{ei} \\ &= \frac{\partial w_C}{\partial \lambda_i} + \frac{\partial w_e}{\partial \lambda_i} \\ &= \frac{G_C}{2} \left( \frac{1 - \delta^2}{(1 - \delta^2 v_2 (D_2 - 3))^2} - \frac{\delta^2}{(1 - \delta^2 v_2 (D_2 - 3))} \right) \cdot [\dot{v}_2 (D_2 - 3) + v_2] \cdot \dot{D}_2 \\ &\quad + \frac{2G_e}{\beta^2} \cdot [\dot{v}_{-\beta} (D_{-\beta} - 3) + v_{-\beta}] \cdot \dot{D}_{-\beta} \end{aligned} \tag{14}$$

for the principal engineering stresses. The reinforcement function  $v_k$  is deliberately kept general. This allows the most general possible characterization of the stress-strain behavior of filled systems. Eq. 14 can be used for the general description of the principal stresses  $P_i$  as well as for the description of an experiment under uni-axial, bi-axial or planar conditions. For the calculation of the principal engineering stresses  $P_i$  the following relations can be derived from Eq. 2.

$$D_k = \sum_{i=1}^3 \lambda_i^k \quad \text{and} \quad \dot{D}_k = k \lambda_i \tag{15}$$

For an experiment carried out under uni-axial conditions, the following relationships apply for deformation in the z-direction  $\lambda_z = \lambda$ ,  $\lambda_x = \lambda^{-0.5}$  and due to incompressibility  $\lambda_y = (\lambda_x \lambda_z)^{-1}$ .

$$D_2 = \lambda^2 + \frac{2}{\lambda}, \quad \dot{D}_2 = 2 \left( \lambda - \frac{1}{\lambda^2} \right), \quad D_{-\beta} = \lambda^{-\beta} + 2\lambda^{\frac{\beta}{2}} \quad \text{and} \quad \dot{D}_{-\beta} = \beta \left( \frac{\lambda^{\frac{\beta}{2}} - \lambda^{-\beta}}{\lambda} \right) \tag{16}$$

When measuring under bi-axial conditions with a force acting in the  $x$  and  $y$  directions ( $\lambda = \lambda_x = \lambda_y$  and  $\lambda_z = (\lambda_x \lambda_y)^{-1}$ ), the calculation of the parameters  $D_k$  and  $\dot{D}_k$  yields the following expressions.

$$D_2 = 2\lambda^2 + \frac{1}{\lambda^4}, \quad \dot{D}_2 = 4 \left( \lambda - \frac{1}{\lambda^5} \right), \quad D_{-\beta} = 2\lambda^{-\beta} + \lambda^{2\beta} \quad \text{and} \quad \dot{D}_{-\beta} = 2\beta \left( \frac{\lambda^{2\beta} - \lambda^{-\beta}}{\lambda} \right) \tag{17}$$

Another possibility to characterize the stress-strain curves in the non-linear deformation range is to measure under pure shear or planar tension. Bergström<sup>4</sup> showed that both measurements yield

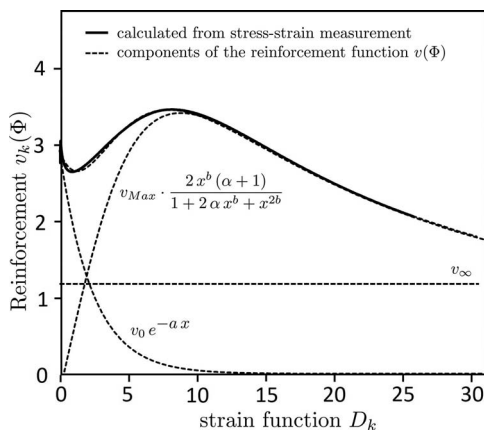


FIG. 1. — Reinforcement  $v(\phi, D_k)$  as a function of the deformation.

comparable results for moderate deformations. Measurements under planar tension are much easier to perform than measurements under pure shear. Therefore we discuss the nonlinear deformation behavior in the experimental part on measurements performed under planar tension as well as uniaxial and bi-axial conditions. For planar tension, the following relationships are found for the parameters  $D_k$  and  $\dot{D}_k$ .

$$D_2 = \lambda^2 + \frac{1}{\lambda^2} + 1, \quad \dot{D}_2 = 2 \left( \lambda - \frac{1}{\lambda^3} \right), \quad D_{-\beta} = \lambda^{-\beta} + \lambda^{\beta} + 1 \quad \text{and} \quad \dot{D}_{-\beta} = \beta \left( \frac{\lambda^{\beta} - \lambda^{-\beta}}{\lambda} \right) \quad (18)$$

The behavior at small deformations can be described by the limiting case  $D_k \rightarrow 3$ . This simplifies Eq. 14 for the limiting case of small deformations.

$$P_i = P_{Ci} + P_{e1} = \frac{G_C}{2} v_2 \dot{D}_2 + \frac{2G_e}{\beta^2} v_{\beta} \dot{D}_{-\beta} \quad (19)$$

For the example of an uni-axial deformation, the combination of Eq. 19 and Eq. 16 yields Hooke's law with a reinforcement factor  $v(\Phi, D_k \rightarrow 3) \rightarrow v(\Phi)$ .

$$P = G_C v(\Phi) \left( \lambda - \frac{1}{\lambda^2} \right) + \frac{2G_e}{\beta} v(\Phi) \left( \frac{\lambda^{\frac{\beta}{2}} - \lambda^{-\beta}}{\lambda} \right) \approx 3 v(\Phi) (G_C + G_e) \varepsilon = v(\Phi) E \cdot \varepsilon \quad (20)$$

Thus, the approach proposed by us in the limiting case of small deformations gives the hydrodynamic amplification, or its general formulation (see Eq. 4).

Figure 1 shows the typical curve of the reinforcement function for a carbon black filled compound (see sample  $C_5$  on table 1). These are discussed explicitly in the experimental section as a function of the type and quantity of filler.

In the following, we would like to suggest a function that we propose for the quantitative description of the deformation dependent reinforcement. This function is made up of three components. For small deformations, a decrease in the reinforcement is observed, which we describe using an exponential function. In the medium deformation range, often a maximum of the reinforcement is observed, which we model using a modified Cole-Cole function. In the case of large deformations, the reinforcement should tend asymptotically towards a constant value, the hydrodynamic reinforcement.

TABLE I  
COMPOSITION OF MODEL COMPOUNDS (UNIT OF VALUES IN PER HUNDRED RUBBER)

Ingredient	C <sub>1</sub>	C <sub>2</sub>	C <sub>3</sub>	C <sub>4</sub>	C <sub>5</sub>	C <sub>6</sub>	C <sub>7</sub>	C <sub>8</sub>	C <sub>9</sub>
Natural rubber SVR CV60	100								
Carbon Black N550	0	30	50	70	85	0			
Carbon Black N220	0					30	45	60	75
Sulfur	4								
CBS	1.4								

The strain-dependent amplification can thus be described quantitatively, with  $v_{Max}$ ,  $v_0$ ,  $v_\infty$ ,  $b$ , and  $\zeta$  as parameters.

$$v_k(x) = v_{Max} \cdot \frac{2x^b(\alpha + 1)}{1 + 2\alpha x^b + x^{2b}} + v_0 e^{-ax} + v_\infty \text{ with } x = \left(\frac{D_k - 3}{\zeta}\right) \text{ and } \alpha = \cos \frac{b\pi}{2} \tag{21}$$

The parameters  $v_0$  and  $\frac{a}{\zeta}$  characterize the decrease of the reinforcement at small strains, the parameters  $\zeta$  and  $v_{Max}$  the position and height of the maximum of the reinforcement. The decrease of the reinforcement at large deformations is characterized by the parameter  $b$ . At very large deformations ( $D_k \rightarrow \infty$ ), the reinforcement approaches the value  $v_\infty$  asymptotically.

To calculate the principal engineering stresses  $P_i$ , the derivative of the reinforcement function  $\dot{v}_k$  according to the strain function  $D_k$  is required (see Eq. 21).

$$\dot{v}_k = \frac{\partial v_k}{\partial D_k} = \frac{1}{\zeta} \left[ v_{Max} \frac{2b(\alpha + 1)x^{b-1}(1 - x^{2b})}{(1 + 2\alpha x^b + x^{2b})^2} - v_0 a e^{-ax} \right] \tag{22}$$

For the limiting case of small deformations ( $x \rightarrow 0$ ), the reinforcement function asymptotically approaches a constant value of  $v_\infty + v_0$ . If a maximum in the reinforcement is formed, it is reached approximately at a deformation of  $D \approx \zeta + 3$  and has the value of  $v_{Max}$ .

The equations derived so far form the basis for the implementation in a finite element program. In our case, a ‘User-Defined Function’ was created in Abacus. The first results are discussed for some of the materials which will be introduced in the following sections. The assumptions and equations on which the implementation is based will be described in a subsequent article.

EXPERIMENTAL INVESTIGATIONS

To determine the reinforcement properties of carbon black using the modified extended tube model METM, nine model compounds were prepared. The formulation details are provided in Table 1. Natural rubber was selected as the base polymer. Each mixture was blended in a 1.5 l internal mixer (GK1.5 Werner & Pfleiderer). Initially, the polymer was introduced, followed by the addition of the filler, which was mixed for an additional 3 min at 50 rpm. Subsequently, sulfur and accelerator were added on an open mill after the mixture was discharged. Test plates with a thickness of 2 mm were vulcanized under pressure (200 bar) at 150 °C for 15 min from all mixtures.

UNFILLED REFERENCE SYSTEM

Compound C<sub>1</sub> serves as the unfilled reference material used as a baseline for determining the network parameters. The solid lines in Figure 2 depict the results of measurements under

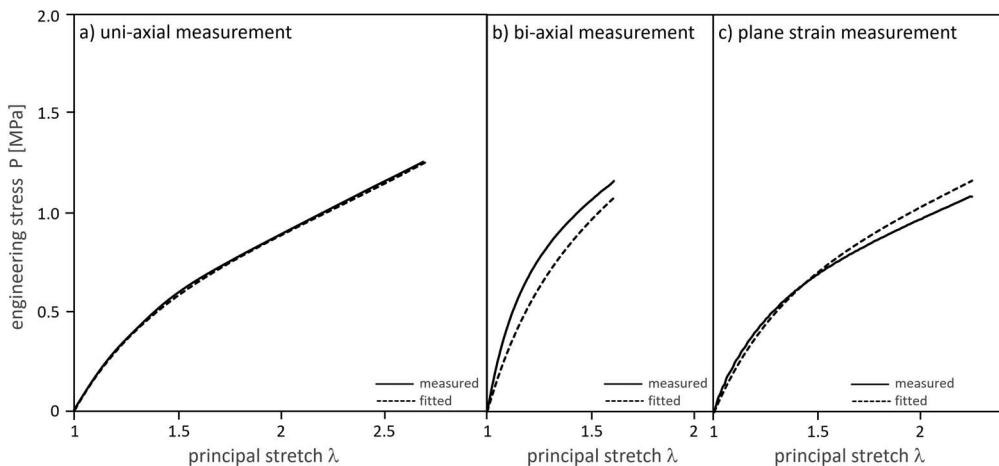


FIG. 2. — Uniaxial (a), biaxial (b), and planar (c) tension measurements of the unfilled reference compound  $C_1$  and the fitting result with the extended tube model.

uniaxial (Figure 2a), biaxial (Figure 2b), and planar (Figure 2c) deformation. The dotted lines represent the fitting of the measured data to the extended tube model (see Eq. 1).

The fitting was conducted simultaneously for the uniaxial, biaxial, and planar measurements. The obtained parameters are summarized in Table 2. The parameter  $\beta$  was set to 0.2 as suggested by Heinrich and Kaliske.<sup>8</sup>

The most significant deviations between the calculated and measured curves are observed in the biaxial experiment. In this case, the measured forces exceed the calculated forces for each deformation. Eberlein<sup>30</sup> demonstrated that this discrepancy arises from stress inhomogeneities occurring during the biaxial test. This issue could potentially be addressed through an optimization process. However, we did not pursue this optimization due to the differing objectives of our study. For the subsequent evaluation of the filled systems, we employed the parameters listed in Table 2.

#### FILLED SYSTEMS

The Figures 3 and 4 show the results of the uni-axial, bi-axial and planar strain measurements of the carbon black-filled samples  $C_1$  to  $C_9$ .

The solid lines represent the measured data, while the dashed lines depict the calculated curves. The calculated curves are based on fitting the measured data to the extended tube model (see Eq. 14). In this process, the network parameters from Table 2 were adopted, with

TABLE II  
RESULT OF THE FIT OF THE EXTENDED TUBE MODEL TO THE  
MEASURED DATA

Parameter	Fitted value
$G_C$ [MPa]	0.2( $\pm$ 0.03)
$G_e$ [MPa]	0.54( $\pm$ 0.03)
$\delta$	0.124( $\pm$ 0.05)

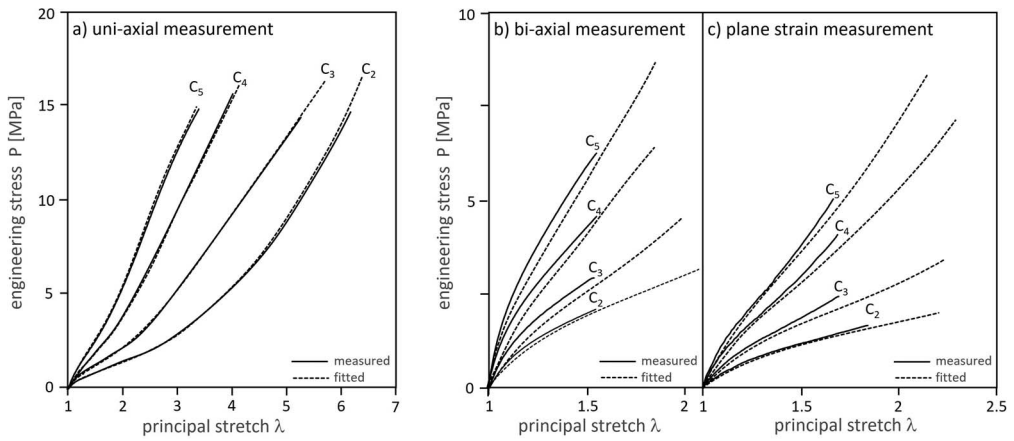


FIG. 3. — Uni- (a), bi-axial (b), and planar tension (c) measurements of the carbon black filled compound (N550)  $C_2 - C_4$ .

only the parameters of the reinforcement function varied. Overall, a very good agreement is observed between the calculated and measured curves.

The fitting process enables the quantification of the reinforcement function. Table 3 presents the parameters of the reinforcement function, and Figure 5 illustrates the graphical representation of the reinforcement function as a function of strain. A quantitative assessment of the reinforcement behavior can be conducted by examining the parameters of the reinforcement function. This can be effectively divided into several areas: reinforcement at small strains ( $\lambda \rightarrow 0$ ), reinforcement in the range of moderate strains, and reinforcement in the range of ultimate properties such as the elongation at break. For small strains ( $D_k \rightarrow 3$ ), the reinforcement function (refer to Eq. 21) approaches asymptotically the value ( $v = v_0 + v_\infty$ ). The left-hand diagram in Figure 6 illustrates this limiting value for the two fillers tested, plotted against the filler’s volume fraction. It also depicts the hydrodynamic reinforcement behavior. The notable enhancement in reinforcement with increasing filler volume fraction

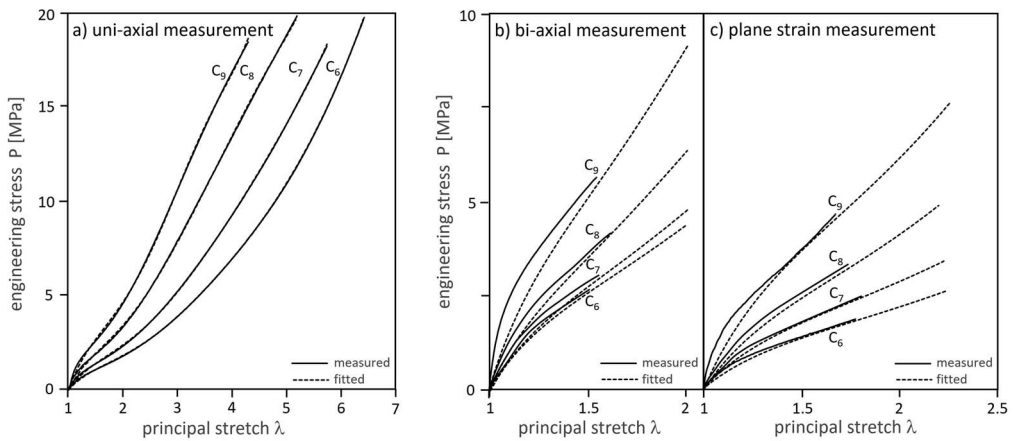


FIG. 4. — Uni- (a), bi-axial (b), and planar tension (c) measurements of the carbon black filled compound (N220)  $C_4 - C_8$ .

TABLE III  
PARAMETERS OF THE REINFORCEMENT FUNCTION  $v$

	$C_2$	$C_3$	$C_4$	$C_5$	$C_6$	$C_7$	$C_8$	$C_9$
$\Phi_F$	0.23	0.33	0.41	0.46	0.23	0.31	0.38	0.43
$v_{Max}$	1.5	2.9	3.8	4.2	1.9	2.7	3.4	3.6
$\zeta$	10.1	6.5	4.7	4	8.7	8.4	6.4	4.9
$b$	1	1	1	1	1	1	1	1
$v_0$	1.9	2.3	4.1	5.0	2.4	3.5	4.9	6.3
$a$	8.3	6.0	4.8	4.2	10.0	8.4	7.7	6.2
$v_\infty$	0.4	0.7	0.8	1.1	0.6	0.2	0.1	0.9

suggests the generation of filler-filler and filler-polymer interactions, likely due to the formation of mechanically unstable filler-polymer-filler clusters.

The decline in reinforcement with increasing deformation in the range of smaller deformations is characterized by the relation (refer to Eq. 21)

$$v_k(D_k \rightarrow 3) \approx v_0 \cdot e^{-\frac{a}{\zeta}(D_k-3)} + v_\infty \quad (23)$$

The diagram on the right in Fig. 7 illustrates the decay parameter  $\frac{a}{\zeta}$  as a function of the volume fraction of the filler. A value close to one is observed for all filling levels and regardless of the filler.

A local maximum of reinforcement is observed in the range of medium deformation. The maximum reinforcement  $v_{Max}$  is depicted in the middle diagram of Fig. 6 as a function of the filler's volume fraction. The deformation at which the reinforcement reaches its local maximum can be determined from the parameter  $\zeta$ , illustrated in the left-hand diagram of Fig. 7.

It's notable that the position of the local maximum decreases linearly with increasing filler volume fraction and lies within a range of 100% to 250% for technically viable filling ratios between 20 phr and 80 phr. A comparable behavior is observed for the two fillers under investigation.

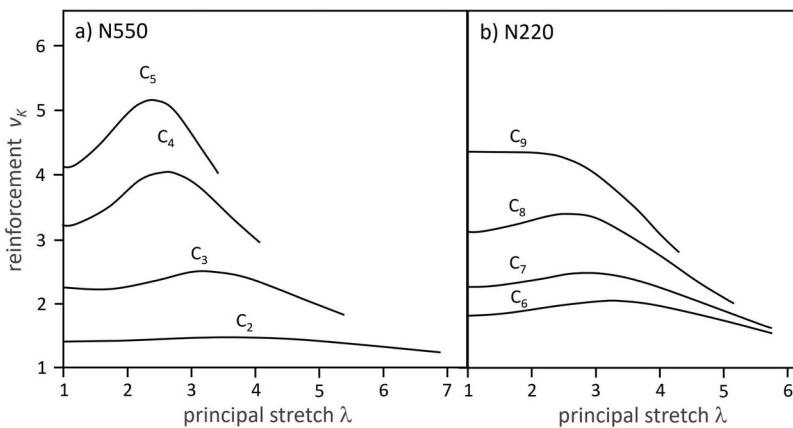


FIG. 5. — Reinforcement function  $v_k(\lambda)$  for the carbon black N550 (a) and N220 (b).

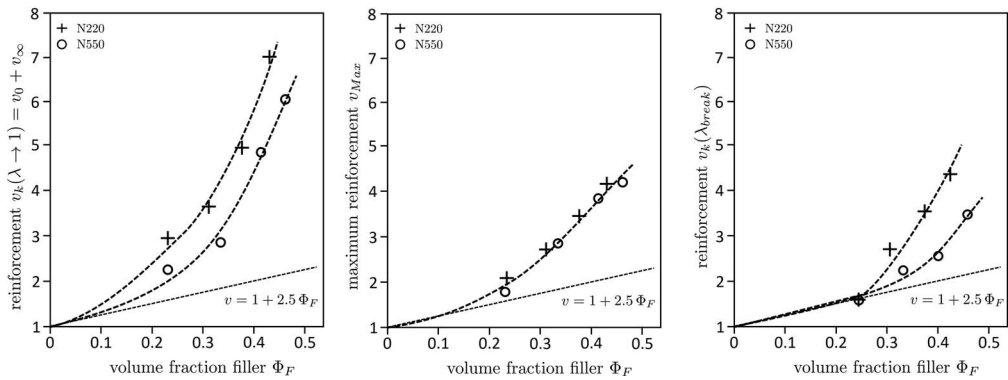


FIG. 6. — Reinforcement  $\nu$  for small, medium, and high deformations.

Even within the medium deformation range, the reinforcement remains significantly higher than the purely hydrodynamic reinforcement (refer to the middle diagram in Fig. 6). This suggests that even in this deformation behavior, the reinforcement is predominantly influenced by the deformation process and the breakup and reformation of filler-polymer-filler clusters.

Given that the determination of the reinforcement at large deformations is constrained by sample fracture, discussing the parameter  $\nu_\infty$  as a function of filling level lacks meaningful quantitative analysis due to the associated measurement error. Instead, we regard the reinforcement at elongation at break as a more meaningful measure of the reinforcement at large deformations. This is depicted in the diagram on the right in Fig. 6.

The reinforcement at elongation at break is still higher than the hydrodynamic reinforcement. This means that even at high deformations, the filler network built from filler-filler and filler-polymer interactions cannot be completely degraded. Comparing the two carbon blacks N220 and N550, one finds significant differences both at small and large deformations. The more active carbon black N220 exhibits higher reinforcements in both areas.

In the left diagram of Figure 7, the term responsible for the decrease in reinforcement at small deformations (see Equation 23), is shown as a function of the filler volume fraction.

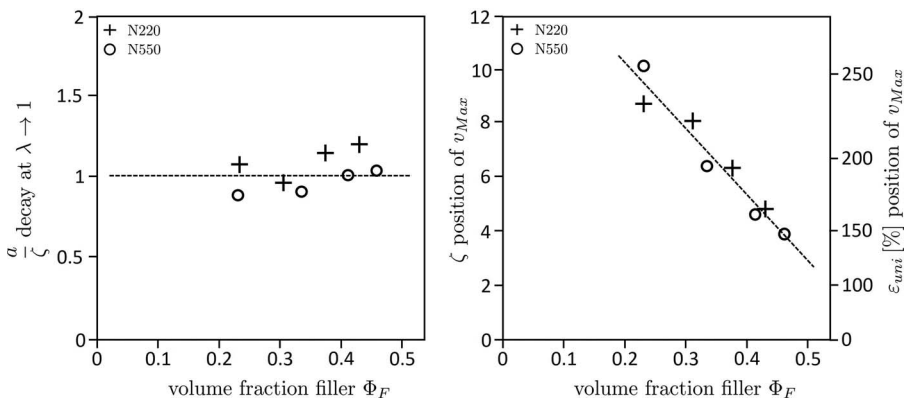


FIG. 7. — Parameters  $\zeta$  and  $\frac{g}{\eta}$  of the reinforcement for small, medium, and high deformation.

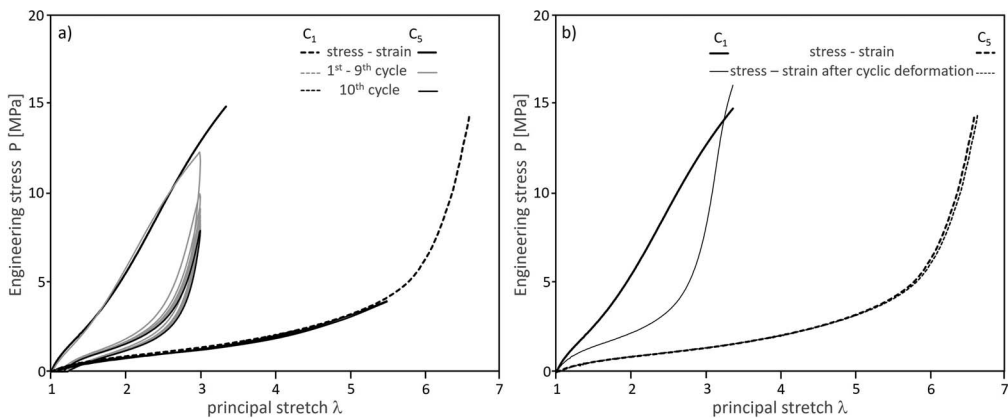


FIG. 8. — Stress-strain curves of a filled ( $C_5$ ) and unfilled ( $C_1$ ) sample before, during (a) and after (b) a 10 fold cyclic deformation at 80% of the elongation at break.

Within the limits of measurement accuracy, it is found that this term is independent of the amount and type of filler and assumes a value of  $\frac{\sigma}{\sigma_0} \approx 1$ .

In the right diagram of Figure 7, the position of the maximum reinforcement as a function of the filler volume fraction is depicted. For better understanding, the deformation for the case of uniaxial deformation is plotted on the right axis. For both fillers, an almost linear shift of the maximum reinforcement to smaller deformations is observed with increasing filler content.

In conclusion, it must be stated that a quantitative interpretation of the data presented in Figures 6 and 7 poses a challenge. Further investigations involving a broader array of fillers are required to draw generalizable conclusions. Nonetheless, the correlations identified thus far suggest that the proposed description of reinforcement behavior via a reinforcement function provides a solid foundation for the quantitative assessment of the mechanical properties of filled elastomers. It can be postulated that the parameters of the reinforcement function facilitate a correlation between the characteristics of the mechanically unstable filler clusters induced by filler-filler or filler-polymer interactions and the macroscopic mechanical properties.

To demonstrate that the effects discussed are indeed solely caused by the filler, as well as filler-filler and filler-polymer interactions, cyclic measurements were conducted on all samples. This type of measurement was first published by Mullins [Mullins, 1969].

In the presented example, S2 rods from the samples were deformed 10 times at 80% of the elongation at break (see the left diagram in Figure 8). The value of 80% was chosen for practical reasons. Experience shows that the samples do not tear during a multiple cyclic deformation when subjected to deformations smaller than to 80% of the elongation of break. After the tenfold cyclic deformation, the S2 samples were removed and remeasured. This is because the thickness and length of the samples can change significantly after cyclic deformation, depending on the formulation of the samples. Finally, another tensile test until failure is conducted on the cyclically pre-deformed samples. The results of these measurements for the unfilled sample  $C_1$  and the filled sample  $C_5$  are shown in the right diagram of Figure 8. For the unfilled sample  $C_1$ , the stress-strain behavior changes only slightly before and after cyclic loading, while the effect on the filled sample  $C_5$  is significant. This altered behavior due to cyclic deformation can be explained solely by the influence of the filler. That is, the clusters formed by filler-filler and filler-polymer interactions are deformed and broken down during cyclic deformation and can partially reform through flocculation.

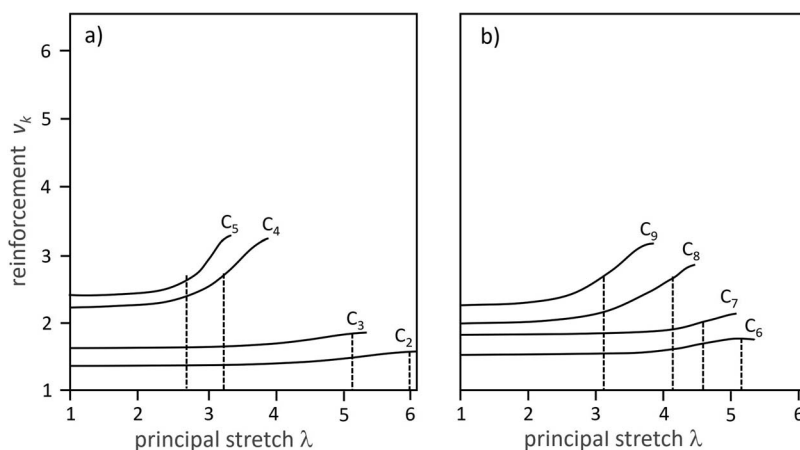


FIG. 9. — Reinforcement function  $v(\lambda)$  for the carbon black N550 (a) and N220 (b) after a 10 fold cyclic pre-deformation.

The cyclic experiments were conducted on all filled systems ( $C_2$  to  $C_9$ ). Subsequently, the measurement curves were fitted with the METM model, without altering the parameters of the polymer network  $G_e$ ,  $G_N$ ,  $\delta$ , and  $\beta$ . This is justified since the cyclic deformation has no or only a negligible small influence on the mechanical behavior of the unfilled sample (see right diagram in 8).

As a result of fitting the cyclically pre-deformed tensile-strain data with the METM model, the reinforcement function for each sample can be calculated. This allows for a detailed analysis of the material behavior under cyclic loading conditions. Thus, with the METM model, the Mullins effect can be quantitatively described. The introduction of the reinforcement function allows for a quantitative description and interpretation of the effect of cyclic deformation on filler-filler and filler-polymer interactions.

In Figure 9, the reinforcement functions of all cyclically pre-deformed samples are summarized. Comparing this with the reinforcement functions of the initial, unaltered samples (see Figure 5), it is observed that the reinforcement of the pre-deformed samples is only increased when subjected to strain levels at or beyond the maximum deformation of the cyclic loading (here 80% of the elongation of break). The dotted lines in Fig. 9 represent the maximum deformation  $v(\lambda) = v_{\text{cycleMax}}$  during the cyclic pre-deformation. At smaller deformations, a nearly constant reinforcement is achieved through the cyclic pre-deformation.

Our measurements substantiate the hypothesis that reinforcement in filled elastomers can be attributed to mechanically unstable filler clusters, which emerge from interactions among fillers and between fillers and the polymer matrix. The larger the filler cluster, the higher the reinforcement at small deformations. Larger clusters are more fragile and therefore break at lower strains. Deformation induces a dynamic equilibrium of breaking and reforming filler clusters, shifting towards smaller cluster sizes with increased deformation. During cyclic deformation, the maximum cluster size is governed by the largest deformation, denoted as  $\lambda_{\text{cyclMax}}$ . Subsequent cyclic deformations lead to a stable distribution of filler clusters, with a maximum cluster size dependent on the largest deformation. The METM model represents this with a reinforcement function that remains constant up to the maximum cyclic deformation, expressed as  $v_k(\lambda) = v(\lambda_{\text{cyclMax}})$  for  $\lambda \leq \lambda_{\text{cyclMax}}$ .

OUTLINE FE IMPLEMENTATION

This section sets basic requirements for a 3D finite element (FE) implementation of the METM expressed by strain energy function Eq. 12. Since the incompressibility constraint  $J := \det \mathbf{F} = 1$  cannot be explicitly fulfilled for a 3D continuum, an extension of the strain energy function  $w(\Phi)$  is introduced that allows the description of compressible material behavior:

$$\begin{aligned}
 w(\Phi) &= w_C + w_e + G(J) \\
 &= \frac{G_C}{2} \left[ \frac{(1 - \delta^2)v(\Phi, D_2)(D_2 - 3)}{(1 - \delta^2v(\Phi, D_2)(D_2 - 3))} + \ln(1 - \delta^2v(\Phi, D_2)(D_2 - 3)) \right] \\
 &\quad + \frac{2G_e}{\beta^2} v(\Phi, D_{-\beta})(D_{-\beta} - 3) + G(J)
 \end{aligned} \tag{24}$$

An initially arbitrary function  $G(J)$  in dependence of Jacobian  $J$  describes the compressible part. Due to physical constraints further limitations hold with respect to  $G(J)$  and  $w(\Phi)$ . The strain energy function needs to fulfill the following limits:

$$\lim_{J \rightarrow 0} w(\Phi) \rightarrow +\infty \quad \text{and} \quad \lim_{J \rightarrow +\infty} w(\Phi) \rightarrow +\infty. \tag{25}$$

Additionally,  $w(\Phi)$  must be zero in the unloaded reference configuration. As shown in literature (Marsden and Hughes,<sup>31</sup> Ciarlet<sup>32</sup>) the limits defined in Eq. 25 are essential for the existence and uniqueness of solutions derived from hyperelastic material models.

It should be mentioned that FE concepts accounting for compressible material behavior such as Kaliske and Heinrich<sup>8</sup> could be applied alternatively.

To fulfill Eq. 25, the compressible part  $G(J)$  in Eq. 24 must be convex. In literature (Ciarlet,<sup>32</sup> Ogden<sup>33</sup>) several Ansatz functions can be found that fulfill this requirement. For the following derivations a specific but admissible form of  $G(J)$  is chosen:

$$G(J) = -\kappa \ln J + \frac{\Lambda}{4} (J^2 - 1 - 2 \ln J). \tag{26}$$

$\Lambda$  in Eq. (26) can be interpreted as *Lamé-constant* and the constant parameter  $\kappa$  is defined as:

$$\kappa = \left[ G_C(1 - \delta^2)v(D_2 = 3) - \frac{2}{\beta} G_e v(D_{-\beta} = 3) \right]. \tag{27}$$

For modeling incompressible material behavior with Eq. (24) by using Eq. (26), the *Lamé-constant*  $\Lambda$  can be interpreted as penalty-parameter, i.e., for sufficiently large values of  $\Lambda$ , the term in brackets tends to zero in Eq. (26), which is corresponding to the incompressibility constraint  $J = 1$ . Eventually, the strain energy density function  $w(\Phi)$  for FE implementation is given in its final form by employing Eq. (26):

$$\begin{aligned}
 w(\Phi) &= \frac{G_C}{2} \left[ \frac{(1 - \delta^2)v(\Phi, D_2)(D_2 - 3)}{(1 - \delta^2v(\Phi, D_2)(D_2 - 3))} + \ln(1 - \delta^2v(\Phi, D_2)(D_2 - 3)) \right] \\
 &\quad + \frac{2G_e}{\beta^2} v(\Phi, D_{-\beta})(D_{-\beta} - 3) - \kappa \ln J + \frac{\Lambda}{4} (J^2 - 1 - 2 \ln J)
 \end{aligned} \tag{28}$$

By means of Eq. (28) the principal stresses can be derived in a similar manner as already shown in section “Analytical derivation of the principal stresses  $P_i$ ”. If a FE implementation in Lagrangian description is pursued, the 2<sup>nd</sup> Piola-Kirchhoff stress tensor  $\mathbf{S}$  is required. It can be derived from  $w(\Phi)$  by the following relation (refer to e.g. Truesdell and Noll<sup>34</sup> for further information):

$$\mathbf{S} = \widehat{\mathbf{S}}(\mathbf{F}) = 2 \frac{\partial w(\Phi)}{\partial \mathbf{C}} \tag{29}$$

The corresponding stress increment  $\Delta \mathbf{S}$  in the reference configuration is given as follows:

$$\begin{aligned} \Delta \mathbf{S} &= \Delta \left( 2 \frac{\partial w(\Phi)}{\partial \mathbf{C}} \right) = \mathcal{L} \frac{1}{2} \Delta \mathbf{C} \\ \text{with } \mathcal{L} &:= 4 \frac{\partial^2 w(\Phi)}{\partial \mathbf{C} \otimes \partial \mathbf{C}}. \end{aligned} \tag{30}$$

The stress increment  $\Delta \mathbf{S}$  is required for the calculation of the consistent linearization of the weak form of equilibrium that underlies the FE implementation. The nonlinear equations in the weak form of equilibrium result from the derivation of stresses from Eq. 28 in Eq. 29. for more information on the subject, the interested reader is referred to Wriggers.<sup>35</sup>

In an equivalent way to strain tensors, a spectral decomposition can be given for stress tensors. For the 2<sup>nd</sup> Piola-Kirchhoff stress tensor this means:

$$\mathbf{S} = \sum_{i=1}^3 S_i \mathbf{N}_i \otimes \mathbf{N}_i. \tag{31}$$

$S_i$  denote the principal stresses of the 2<sup>nd</sup> Piola-Kirchhoff stress tensor, whereas  $N_i$  indicate unit vectors of an orthogonal eigenvector base. Numerically, the eigenvectors  $N_i$  are determined by solving the following eigenvalue problem:

$$(\mathbf{S} - S_i \mathbf{1}) \mathbf{N}_{(i)} = 0. \tag{32}$$

More elaborate is the representation of the material tensor  $\mathcal{L}$  from Eq. 30<sub>2</sub> in principal axes. In Chadwick and Ogden<sup>36</sup> the related form was derived as:

$$\begin{aligned} \mathcal{L} &= \sum_{i=1}^3 \sum_{j=1}^3 L_{ijij} \mathbf{N}_i \otimes \mathbf{N}_i \otimes \mathbf{N}_j \otimes \mathbf{N}_j \\ &+ \frac{1}{2} \sum_{i \neq j} L_{ijij} (\mathbf{N}_i \otimes \mathbf{N}_j \otimes \mathbf{N}_i \otimes \mathbf{N}_j + \mathbf{N}_i \otimes \mathbf{N}_j \otimes \mathbf{N}_j \otimes \mathbf{N}_i). \end{aligned} \tag{33}$$

In accordance to Eq. 29 and Eq. 30, the corresponding components in principal directions are obtained as:

$$S_i = 2 \frac{\partial w(\Phi)}{\partial C_i}; \quad L_{ijij} = 2 \frac{\partial S_i}{\partial C_j}; \quad L_{ijij} = \frac{S_i - S_j}{C_i - C_j}. \tag{34}$$

Eqs. 34 can further be modified in terms of principal stretches  $\lambda_i$  by employing:

$$C_i = \lambda_i^2 \quad \Rightarrow \quad \frac{\partial(\dots)}{\partial C_i} = \frac{1}{2 \lambda_i} \frac{\partial(\dots)}{\partial \lambda_i} \tag{35}$$

and therefore

$$S_i = \frac{1}{\lambda_i} \frac{\partial w(\Phi)}{\partial \lambda_i}; \quad L_{ijij} = \frac{1}{\lambda_j} \frac{\partial}{\partial \lambda_j} \left( \frac{1}{\lambda_i} \frac{\partial w(\Phi)}{\partial \lambda_i} \right); \quad L_{ijij} = \frac{S_i - S_j}{\lambda_i^2 - \lambda_j^2}. \tag{36}$$

It must be noted that due to symmetry of the 2<sup>nd</sup> Piola-Kirchhoff stress tensor  $\mathbf{S}$  and the right Cauch–Green tensor  $\mathbf{C}$  as well as the elastic potential character of the strain energy function  $w(\Phi)$ , the following symmetry conditions must hold for the material tensor  $\mathcal{L}$ :

$$L_{ijkl} = L_{jikl} = L_{ijlk} = L_{klij}. \quad (37)$$

For the special case of two or three principal stretches  $\lambda_i$  having an identical value, the components  $L_{ijij}$  are indefinite in Eq. 36. By means of the *L' Hospital* rule, a limit value formation is performed by Chadwick and Ogden:<sup>37</sup>

$$\lim_{\lambda_i \rightarrow \lambda_j} L^{ijij} = \frac{1}{2} (L^{iiii} - L^{iijj}). \quad (38)$$

This completes the derivation of the material tensor  $\mathcal{L}$  in principal axes and the outline of a Lagrangian finite element description and implementation of the material model characterized by the strain energy function in Eq. 28. Since stresses and material tensor are given in principal axes directions, a transformation from arbitrary strain and stress states to principal axes must be performed first. After computing the principal stresses and the components of the material tensor as shown above, a return transformation must follow. The corresponding transformation procedure is explained in, e.g. Reese and Wriggers.<sup>38</sup> For the subsequent numerical examples, the FE implementation was done within Abaqus Standard<sup>10</sup> as user material subroutine.

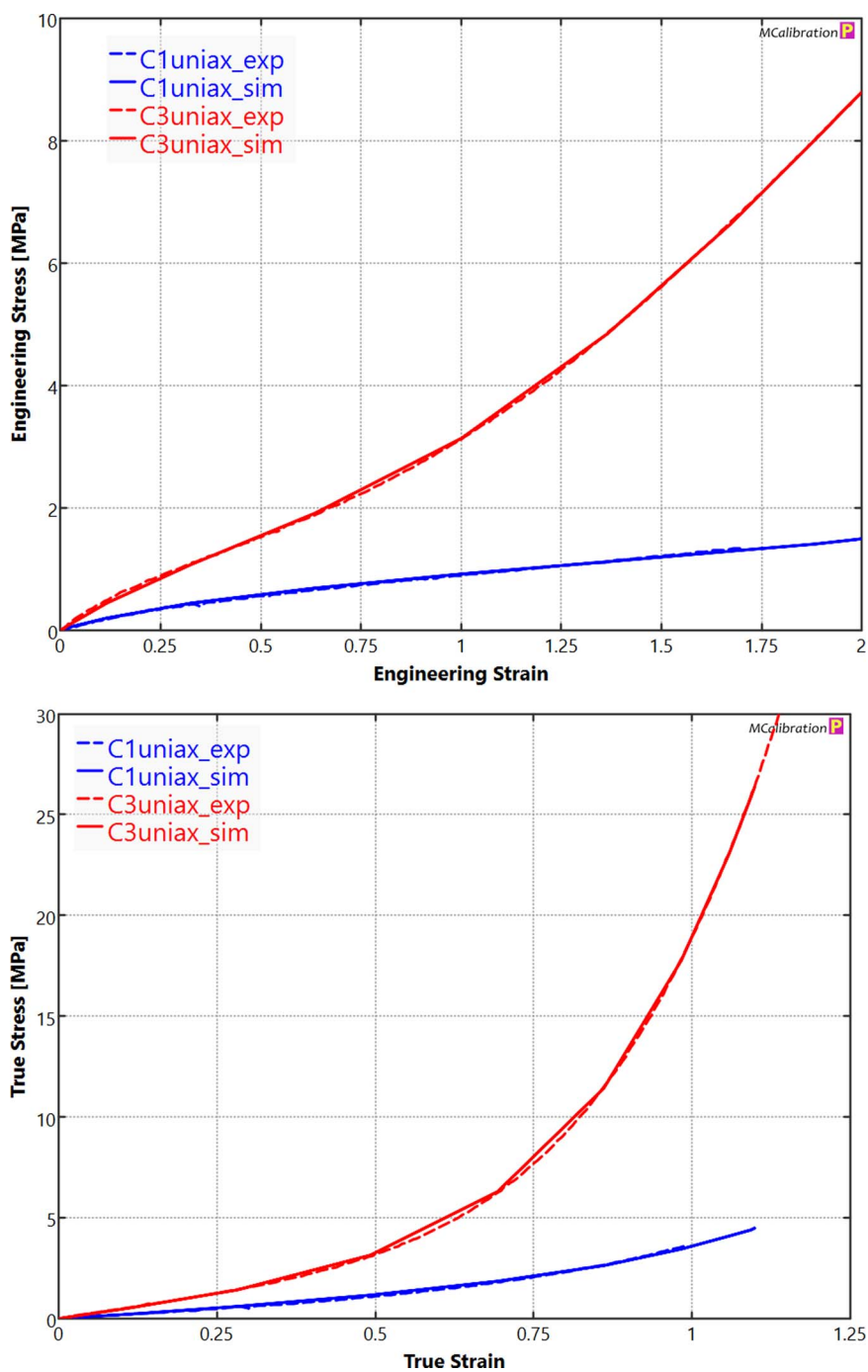
As numerical example for the METM, the uni-axial tension experiment is computed for vulcanizates of the unfilled  $C_1$  and the filled  $C_3$  compounds as reported in table 1. For the FE simulation the material parameters are chosen as given in table 2 ( $C_1$  and  $C_3$ ) and table 3 (reinforcement of  $C_3$ ), respectively. The *Lamé-constant* in both cases is set to  $\Lambda = 10^4$ . The numerical results in Figure 10 replicate the calibrated data for unfilled and filled vulcanizates as reported for  $C_1$  in Figure 2 (a). It should be noted that due to the quasi-incompressible material behavior of the unfilled and filled rubber materials, a hybrid finite element formulation for linear 8-node brick elements was chosen.

The simulated stress-strain curves depicted in Figure 10 can be achieved from different FE models that can ensure an homogeneous stress state in uni-axial tension. Figure 11 depicts two admissible FE models. In Figure 11 (a) just a single element is used with boundary conditions enabling an uni-axial tension stress state. As alternative a complete testing specimen could be modeled according to the experimental setup as shown in Figure 11 (b). The red color in the narrow part of the probe indicates that the same stress in loading direction is achieved as in Figure 11 (a) but at a much higher computational cost. However, the model in Figure 11 (b) can also analyze inhomogeneous stress states in the testing specimen near the clamping plates, if these are of any interest.

#### SUMMARY AND OUTLOOK

The objective of our research was to develop a material model for filled vulcanizates that is physically motivated. This model is based on the extended tube model and has been integrated into a finite element program.

We have demonstrated that the concept of intrinsic deformation cannot be utilized to describe the nonlinear deformation behavior when assuming incompressible, isotropic material behavior. We suggest an alternative method where the principal strains are not directly used, but rather a strain function  $D_k$  is employed to characterize the reinforcement behavior. The reinforcement  $v_k(\phi, D_k)$  is then dependent on this function and the filler's volume fraction. The strain function  $D_k$  corresponds to the first invariant of the right Cauchy-Green tensor  $\mathbf{C}$  across a broad range of deformations. It is only at small deformations that the contribution of the entanglements must be accounted for by an additional reinforcement term  $v_{-\beta}(\Phi, D_{-\beta})$ .

FIG. 10. — Stress-strain curves at initial uni-axial tension loading for  $C_1$  and  $C_3$  vulcanizates.

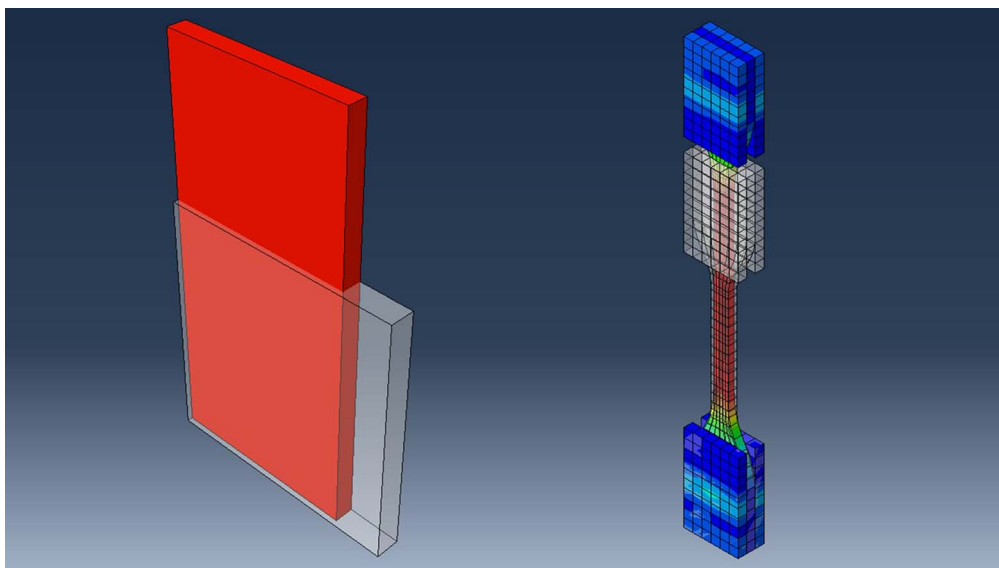


FIG. 11. — Von Mises stress distribution in FE models for uni-axial tension loading of  $C_3$  vulcanizate at identical deformation state; (a) single element, (b) discretization of testing specimen.

We have shown that the reinforcement function can be expressed as the sum of three components that describe the reinforcement at low, medium, and high strains. Comparison with experimental data revealed that the Modified Extended Tube Model (METM) is highly effective in describing the stress–strain behavior of filled systems throughout the entire range of deformation. Moreover, the parameters of the reinforcement function, as determined by fitting the METM to experimental data, can be used to quantitatively describe the reinforcing behavior of the fillers employed.

By analyzing cyclic pre-deformed stress-strain data, we could demonstrate that the parameters of the reinforcement function uniquely characterize the properties of the filler, whereas those of the extended tube model represent the network properties. This indicates that our methodology allows for a quantitative differentiation between network properties and filler-filler and filler-polymer interactions.

Ultimately, we demonstrated that the METM can be integrated into a finite element (FE) routine by incorporating a function that characterizes compressibility, considering the reinforcement function.

Finite element simulation tests of a uniaxial tensile test revealed a close correlation between the simulated and experimental tensile strain curves for both unfilled and filled samples. This convincingly illustrates that the METM approach, which is grounded in physical principles, is highly effective for simulating filled elastomer systems. Looking forward, we aim to enhance the METM model to enable it to capture the cyclic deformation behavior observed during repeated cyclic loading.

#### ACKNOWLEDGEMENT

The financial support for this research by Innosuisse - Swiss Innovation Agency, under grant No 102.422.1 IP-ENG is gratefully acknowledged.

## REFERENCES

- <sup>1</sup>A. Ansari-Benam, A. Bucchi, C. O. Horgan, and G. Saccomandi, Assessment of a new isotropic hyperelastic constitutive model for a range of rubberlike materials and deformations. *Rubber Chemistry and Technology*. **95**, 200–217 (2021).
- <sup>2</sup>L. Costecalde, A. Leygue, M. Coret, and E. Verron, Data-driven identification of hyperelastic models by measuring the strain energy density field. *Rubber Chemistry and Technology*. **96**, 443–454 (2023).
- <sup>3</sup>X. Wan, Y. Zhang, Q. Zhang, L. Zhang, and F. Li, User subroutines platform development for rubber hyperelastic constitutive models and its application in finite element analysis. *Computational Materials Science*. **237**, 112885 (2024).
- <sup>4</sup>J. Bergström, *Mechanics of Solid Polymers*; Elsevier, (2015).
- <sup>5</sup>H. Dal, K. Acikgöz, and Y. Badienia, On the Performance of Isotropic Hyperelastic Constitutive Models for Rubber-Like Materials: A State of the Art Review. *Applied Mechanics Reviews*. **73**, 020802 (2021).
- <sup>6</sup>H. He, Q. Zhang, Y. Zhang, J. Chen, L. Zhang, and F. Li, A comparative study of 85 hyperelastic constitutive models for both unfilled rubber and highly filled rubber nanocomposite material. *Nano Materials Science*. **4**, 64–82 (2022), Trends in Nanomaterials and Nanocomposites: Fundamentals, Modelling and Applications - Part A.
- <sup>7</sup>G. Heinrich, and M. Kaliske, Theoretical and numerical formulation of a molecular based constitutive tube-model of rubber elasticity. *Computational and Theoretical Polymer Science*. **7**, 227–241 (1997).
- <sup>8</sup>M. Kaliske and G. Heinrich, An extended tube-model for rubber elasticity: statistical-mechanical theory and finite element implementation. *Rubber Chem. Tech.*, **72**, 603–632 (1999).
- <sup>9</sup>G. Marckmann and E. Verron, Comparison of Hyperelastic Models for Rubber-Like Materials. *Rubber Chemistry and Technology*. **79**, 835–858 (2006).
- <sup>10</sup>Abaqus. <https://www.3ds.com/products/simulia/abaqus>.
- <sup>11</sup>Ansys. <https://www.ansys.com>.
- <sup>12</sup>R. G. Treloar, *The Physics of Rubber Elasticity*; Clarendon Press, (1975).
- <sup>13</sup>M. Mooney, A theory of large elastic deformation. *Journal of Applied Physics*. **11**, 582–592 (1940).
- <sup>14</sup>R. Rivlin, Large elastic deformations of isotropic materials. IV. Further developments of the general theory. *Philosophical Transactions of the Royal Society of London. Series A, Mathematical and Physical Sciences*. **241**, 379–397 (1948).
- <sup>15</sup>R. W. Ogden, *Non-linear elastic deformations*; Dover Publications, (1997).
- <sup>16</sup>O. Yeoh, Some forms of the strain energy function for rubber. *Rubber Chem. Tech.*, **66**, 754–771 (1993).
- <sup>17</sup>T. A. Vilgis, G. Heinrich, and M. Klüppel, *Reinforcement of Polymer Nano-Composites: Theory, Experiments and Applications*; Cambridge University Press, (2009).
- <sup>18</sup>M. Klüppel and J. Schramm, A generalized tube model of rubber elasticity and stress softening of filler reinforced elastomer systems. *Macromol. Theory Simul.* **9**, 742–754 (2000).
- <sup>19</sup>H. Lorenz, M. Klüppel, and G. Heinrich, Microstructure-based modelling and FE implementation of filler-induced stress softening and hysteresis of reinforced rubbers. *ZAMM - Journal of Applied Mathematics and Mechanics/Zeitschrift für Angewandte Mathematik und Mechanik*. **92**, 608–631 (2012).
- <sup>20</sup>G. Heinrich and T. Vilgis, A. Contribution of entanglements to the mechanical properties of carbon black-filled polymer networks. *Macromolecules*. **26**, 1109–1119 (1993).
- <sup>21</sup>J. Bastide and C. Picot, Candau, S. *Macromol. Sci. Phys.*, **19** (1981).
- <sup>22</sup>E. Guth and O. Gold, *Phys. Rev.*, **53**, 322 (1938).
- <sup>23</sup>A. Einstein, *Annalen der Physik*. **19**, 289 (1906).
- <sup>24</sup>A. Einstein, *Annalen der Physik*. **34**, 591 (1911).
- <sup>25</sup>J. Domurath, M. Saphiannikova, and G. Heinrich, The Concept of hydrodynamic Amplification in filled Elastomers. *Kautschuk Gummi Kunststoffe*. **1–2**, 40–43 (2017).
- <sup>26</sup>E. Straube and D. Matzen, *Kautschuk Gummi Kunststoffe*. **45**, 264 (1992).
- <sup>27</sup>R. Christensen, *Mechanics of Composite Materials*; Wiley, (1979).

- <sup>28</sup>J. Bergström, Large Strain Time-Dependent Behavior of Elastomeric Materials. Ph.D. thesis, Massachusetts Institute of Technology, (1999).
- <sup>29</sup>C. Wrana, *Polymerphysik*; Springer, (2014).
- <sup>30</sup>R. Eberlein and S. Holenstein, Efficient material parameter calibration of elastomer specimen in uniaxial tension, planar shear and equibiaxial tension. *Kautschuk Gummi Kunststoffe*. **7–8**, 36–40 (2018).
- <sup>31</sup>J. E. Marsden and T. J. R. Hughes, *Mathematical Foundations of Elasticity*; Prentice–Hall: Englewood Cliffs, NJ, (1983).
- <sup>32</sup>P. G. Ciarlet, *Mathematical Elasticity*; Elsevier: Amsterdam, Vol. I: Three–Dimensional Elasticity (1988).
- <sup>33</sup>R. W. Ogden, Large Deformation Isotropic Elasticity: On the Correlation of Theory and Experiment for Compressible Rubberlike Solids. *Proc. R. Soc. Lond. A*. **328**, 567–583 (1972).
- <sup>34</sup>C. Truesdell and W. Noll, *The Nonlinear Field Theories of Mechanics*; Handbuch der Physik; Springer: Berlin, Vol. **III/3** (1965).
- <sup>35</sup>P. Wriggers, *Nonlinear Finite Element Methods*; Springer: Berlin Heidelberg, (2008).
- <sup>36</sup>P. Chadwick and R. W. Ogden, On the Definition of Elastic Moduli. *Arch. Rat. Mech. Anal.*, **44**, 41–53 (1971A).
- <sup>37</sup>P. Chadwick and R. W. Ogden, W. A Theorem of Tensor Calculus and its Application to Isotropic Elasticity. *Arch. Rat. Mech. Anal.*, **44**, 54–68 (1971B).
- <sup>38</sup>R. Reese and P. Wriggers, A Finite Element Method for Stability Problems in Finite Elasticity. *Int. J. Num. Meth. Eng.*, **38**, 1171–1200 (1995).

[Received May 2024, Revised July 2024]